STUDIES ON TORSION VIBRATION OF A DOUBLE CARDAN JOINT DRIVELINE

SAMEKO Project Report
February 2003

Jussi Sopanen

Department of Mechanical Engineering
Lappeenranta University of Technology
Skinnarilankatu 34
53851 Lappeenranta, Finland
Email: jsopanen@lut.fi

ABSTRACT

Two models of a double cardan joint driveline are presented in this study. A simple analytical model is derived using a multibody dynamics formulation. Another model, which is implemented in a commercial multibody dynamics software application, includes non-linear descriptions of bearing forces in cardan joints. Both include descriptions of the flexibility of the intermediate shaft. These models are used in a co-simulation with a permanent magnet synchronous electric motor (PMSM). Mechanical and electrical non-idealities affecting to the dynamics of the driveline are studied. Modeled non-idealities include unequal joint angles, incorrect phasing of the cardan joints, bearing clearance and current measurement error in the electric motor. The results obtained from two cardan shaft models are compared and a good agreement is obtained. The results show that the electric motor tries to correct the transmission error caused by the mechanical non-idealities. This in turn leads to fluctuating torque and undesirable dynamic loads.

1 INTRODUCTION

The cardan joint, also known as the Hooke's joint or universal joint has been widely used in industrial applications and in automobile drivelines. The cardan coupling is used to connect two intersecting shafts, however, the angular velocity ratio of the two shafts is not constant. The velocity relationship is a function of the joint angle and the rotation angle of the driver. Usually, two cardan joints are connected in such a way that the uneven velocity ratio of the first coupling is cancelled out by the second. However, velocity the intermediate shaft in a double cardan joint driveline is not constant.

Fischer and Paul [1] studied velocity ratios of a double cardan joint both analytically and experimentally. They found that the relative phase angle is the most important variable affecting to the input-output displacement relationship of the double cardan shaft. The relative phase angle is defined as follows: If we consider two planes, one is the plane formed by the input and intermediate shafts and another is formed by output and the intermediate shafts. The angle between these two planes is called the *angle of twist*. The *phase angle* is the angle between two yokes on the intermediate shafts. The *relative phase angle* is the difference between the *phase angle* and the *angle of twist.* Fischer and Paul concluded that the fluctuations in input and output displacements vanish when the joint angles of two joints are equal and the relative phase angle is

set to zero. When the two joint angles are unequal some fluctuation will exist. However, the fluctuation is minimized when the relative phase angle is zero. Sheu et al. [2] studied joint bearing friction in the universal joints. They found that the intermediate shaft of the double cardan joint suffers from bending moments induced by joint friction and velocity fluctuations in the joints. These factors distort the linear relationship between the input and output shafts, even if the joint angles are equal. Fischer and de Waal [3] studied experimentally axial forces in the intermediate joint. They mounted strain gages on the surfaces of the yoke arms. They found that torque causes inward bending of the yoke arms and increasing speed causes them to bend outward. As a result, bending of the yoke arms causes non-negligible axial forces to the cardan joint. Brutti et al. [4] derived a closed form solution for the torque analysis of the double cardan joint. Their model included masses and mass moments of inertia of the links. The effect of flexibility of the intermediate shaft was studied using multibody approach. They concluded that within normal conditions, the effect of elasticity on the input torque is small. However, at higher speed, there is significant difference between the results obtained from rigid and flexible models.

In this paper, dynamics of a double cardan joint is studied together with the model of permanent magnet synchronous motor. Two models of the double cardan joint driveline are presented and the results obtained from them are compared. This paper is organized as follows: in section 2 two different cardan shaft models are introduced. Simulation results are presented in section 3. Finally, summary and conclusions are drawn in section 4.

2 DOUBLE CARDAN SHAFT MODELS

Two models of double cardan joint driveline are presented in this section. The first one is a simple analytical model that can be implemented in a mathematic program, such as Matlab/Simulink. The second model is implemented in a commercial multibody software application (MSC.ADAMS) and this model includes nonlinear descriptions of the bearing forces in the universal joint. The intermediate shaft of the driveline is modeled as flexible in both models; however, the different approaches are used in these models.

2.1 Analytical Model of the Double Cardan Joint Driveline

The model of a cardan driveline is shown in Figure 1. The model consists of four parts that are described by mass moments of inertia (J_i). Each part have one rotational degree-of-freedom (q_i). Therefore, the vector of generalized coordinates can be written as

$$\mathbf{q} = \begin{bmatrix} q_1 & q_2 & q_3 & q_4 \end{bmatrix}^T \tag{1}$$

By using Lagrange's equation, the system equation of motion can be written as follows [5]

$$\mathbf{M}\ddot{\mathbf{q}} + \mathbf{C}_\mathbf{q}^{\ T}\boldsymbol{\lambda} = \mathbf{Q}_e + \mathbf{Q}_f, \tag{2}$$

where $\mathbf{M}$ is the mass matrix, $\mathbf{C}_\mathbf{q}$ is the constraint Jacobian matrix, $\boldsymbol{\lambda}$ is the vector of Lagrange multipliers, $\mathbf{Q}_e$ is the vector of elastic forces and $\mathbf{Q}_f$ is the vector of external forces.

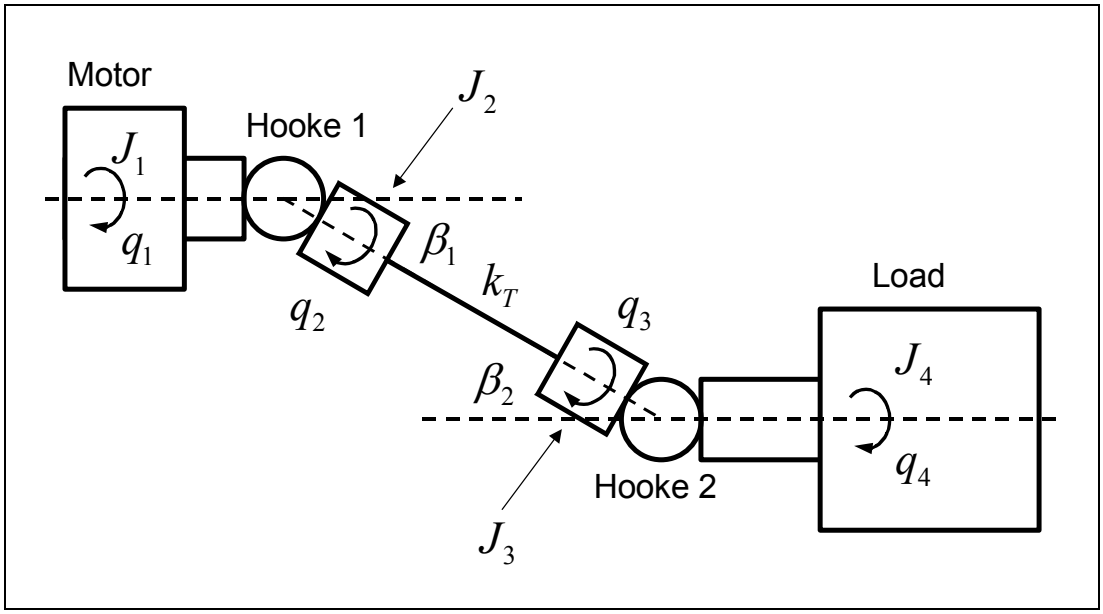

Figure 1. Double cardan joint model.

The mass matrix of the system can be written as follows

$$\mathbf{M} = \begin{bmatrix} J_1 & 0 & 0 & 0 \\ 0 & J_2 & 0 & 0 \\ 0 & 0 & J_3 & 0 \\ 0 & 0 & 0 & J_4 \end{bmatrix}. \tag{3}$$

Kinematical constraints of the Hooke joints can be written as [6]

$$C_1: \quad q_2 - \tan^{-1}\left(\frac{\tan q_1}{\cos \beta_1}\right) = 0 \tag{4}$$

$$C_2: \quad q_4 - \tan^{-1}\left(\frac{\tan q_3}{\cos \beta_2}\right) = 0 \tag{5}$$

The constraint Jacobian matrix is obtained by differentiating the constraint equations with respect to the generalized coordinates

$$\mathbf{C}_{\mathbf{q}} = \frac{\partial \mathbf{C}}{\partial \mathbf{q}} \tag{6}$$

In this case, the constraint Jacobian matrix can be written as follows

$$\mathbf{C}_{\mathbf{q}} = \begin{bmatrix} -\dfrac{\cos\beta_1}{\cos^2 q_1\left(\cos^2\beta_1 - 1\right)+1} & 1 & 0 & 0 \\ 0 & 0 & -\dfrac{\cos\beta_2}{\cos^2 q_3\left(\cos^2\beta_2 - 1\right)+1} & 1 \end{bmatrix} \tag{7}$$

Vector of elastic and damping forces can be written as

$$\begin{aligned} \mathbf{Q}_e = &-\begin{bmatrix} 0 & k_T\left(q_2 - q_3 + \phi\right) & k_T\left(-q_2 + q_3 - \phi\right) & 0 \end{bmatrix}^T \\ &-\begin{bmatrix} 0 & c_T\left(\dot{q}_2 - \dot{q}_3\right) & c_T\left(-\dot{q}_2 + \dot{q}_3\right) & 0 \end{bmatrix}^T \end{aligned} \tag{8}$$

where k_T and c_T are the torsion spring and damping constants and the angle ϕ is the phase angle between the joints in the intermediate shaft. When the phase angle is 90°, the double cardan joint driveline operates as a constant velocity coupling. Physically this means that the angle between the yokes in the intermediate shaft is 0°. The torsion spring constant can be written as

$$k_T = \frac{GI_{xx}}{L} \tag{9}$$

where G is the modulus of the rigidity of the material, I_{xx} and L are the torsion constant and the length of the shaft, respectively.

Equation (2) represents the dynamic equations of the constrained system. These equations are nonlinear and a closed-form solution is often difficult to obtain. The equations can be solved as follows. First, the constraint equations are differentiated twice with respect to time [5]

$$\mathbf{C}_{\mathbf{q}}\ddot{\mathbf{q}} = -\mathbf{C}_{tt} - (\mathbf{C}_{\mathbf{q}}\dot{\mathbf{q}})_{\mathbf{q}}\dot{\mathbf{q}} - 2\mathbf{C}_{\mathbf{q}t}\dot{\mathbf{q}} \tag{10}$$

When the constraints are not dependent on time, Equation (10) can be written as

$$\mathbf{C}_{\mathbf{q}}\ddot{\mathbf{q}} = -(\mathbf{C}_{\mathbf{q}}\dot{\mathbf{q}})_{\mathbf{q}}\dot{\mathbf{q}} \tag{11}$$

By defining the vector $\mathbf{Q}_c$ as

$$\mathbf{Q}_c = \mathbf{C}_{\mathbf{q}}\ddot{\mathbf{q}} = -(\mathbf{C}_{\mathbf{q}}\dot{\mathbf{q}})_{\mathbf{q}}\dot{\mathbf{q}} \tag{12}$$

For a double cardan joint driveline the vector $\mathbf{Q}_c$ can be written as follows

$$\mathbf{Q}_c = \begin{bmatrix} \dfrac{2\sin q_1 \cos q_1 \cos \beta_1 \left(\cos^2 \beta_1 - 1\right)\dot{q}_1}{\left(\cos^2 q_1 \left(\cos^2 \beta_1 - 1\right) + 1\right)^2} \\ \dfrac{2\sin q_3 \cos q_3 \cos \beta_2 \left(\cos^2 \beta_2 - 1\right)\dot{q}_3}{\left(\cos^2 q_3 \left(\cos^2 \beta_2 - 1\right) + 1\right)^2} \end{bmatrix} \tag{13}$$

Equations (2) and (12) can then be combined to one matrix equation as

$$\begin{bmatrix} \mathbf{M} & \mathbf{C_q}^T \\ \mathbf{C_q} & \mathbf{0} \end{bmatrix} \begin{bmatrix} \ddot{\mathbf{q}} \\ \boldsymbol{\lambda} \end{bmatrix} = \begin{bmatrix} \mathbf{Q}_e + \mathbf{Q}_f \\ \mathbf{Q}_c \end{bmatrix} \tag{14}$$

The acceleration vector and the vector of Lagrange multipliers can then be solved from Equation (14). It must be noted that degrees of freedom in the above mentioned model could be easily increased by defining more parts and spring forces that connect them. By this way, more torsion modes could be described. This analytical model can describe the effect of unequal joint angles and incorrect phasing of the joints.

2.2 ADAMS Model of the Double Cardan Joint Driveline

In the ADAMS model, the input and output shafts are connected to ground with revolute joints. The model of the joints and modeling of flexible intermediate shaft is described in following sections.

Model of the Universal Joint

Mathematical models of universal joints are available in commercial multibody dynamics software applications. However, these joints are ideal and described using constraint equations. Thus, non-idealities of the joint, caused by the manufacturing errors or bearing clearance, are not possible to take into account. In order to model the non-idealities of the universal joint, the yokes and the cross are modeled separately as shown in Figure 2. The bearings between the yokes and the cross part are described with non-linear contact forces.

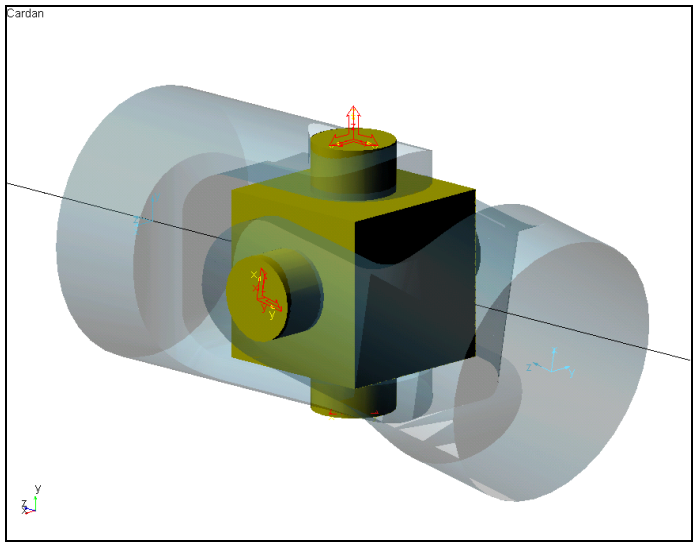

Figure 2. Universal joint modeled with rigid bodies and bearing forces.

The contact force of a bearing is described as a cylinder-in-cylinder contact shown in Figure 3. The coordinate system of the bearing is defined as follows: *Z*-coordinate is oriented along bearing axis and *X*- and *Y*-coordinates are oriented in radial direction. The radial contact force affecting to the shaft is a function of the contact penetration and the penetration velocity and it can be described as follows

$$F_r = -1.0 \cdot \max \begin{cases} K(e_r - c_d)^e + step(e_r, c_d, 0, d, C) \cdot \dot{e}_r \\ 0.0 \end{cases} \tag{15}$$

where K and C are the stiffness and damping constants of the contact and e is the exponent of the force-deflection relationship. Radial displacement e_r and velocity $\dot{e}_r$ between the shaft and sleeve can be obtained from the displacements along X and Y axes as follows

$$e_r = \sqrt{e_x^{\,2} + e_y^{\,2}} \tag{16}$$

$$\dot{e}_r = \frac{2e_x\dot{e}_x + 2e_y\dot{e}_y}{2\sqrt{e_x^{\,2} + e_y^{\,2}}} \tag{17}$$

Clearance in the bearing, c_d, is obtained from radiuses of the cylinders as follows

$$c_d = R - r \tag{18}$$

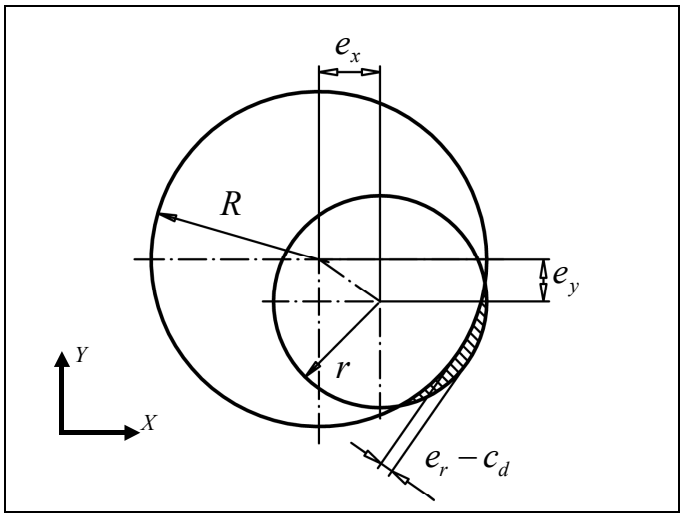

Figure 3. Cylinder-in-cylinder contact.

To prevent a discontinuity in the damping force at contact, the damping coefficient is a cubic step function of the penetration. Thus, at zero penetration, the damping coefficient, *C*, is always zero. The parameter *d* in Equation (15) is the radial displacement e_r when a maximum damping coefficient value is achieved. The *step* function approximates the Heaviside step function with cubic polynomials. It is continuous for first derivatives and it is defined as

$$step(g, g_0, h_0, g_1, h_1) = \begin{cases} h_0 & ;\ g \le g_0 \\ h_0 + \Delta h \cdot \Delta g^2 (3 - 2\Delta g) & ;\ g_0 < g < g_1 \\ h_1 & ;\ g \ge g_1 \end{cases} \tag{19}$$

where $\Delta h = h_1 - h_0$ and $\Delta g = \dfrac{g - g_0}{g_1 - g_0}$. The variable g is the independent variable, g_0 and g_1 are the beginning and ending values of the step. Correspondingly, h_0 and h_1 are the initial and final value of the function.

The radial contact forces in *X* and *Y* directions are obtained as follows

$$F_x = F_r \cos\theta \tag{20}$$

$$F_y = F_r \sin\theta \tag{21}$$

where the attitude angle θ is defined as

$$\theta = \tan^{-1}\left(\frac{e_y}{e_x}\right) \tag{22}$$

An axial force, F_z, in the bearing is described by linear spring-damper force. The model of the universal joint contains three rigid bodies that are connected with four bearing forces. The joint module is attached to shafts with fixed joints.

Flexible Intermediate Shafts

In the ADAMS model, the flexibility of the intermediate shaft is described using a floating frame of reference formulation [5]. In this method, a body reference frame describes rigid body motion and linear elastic deformation is described relative to this frame. Deformation of the body is described by superposition of the vibration modes that are obtained from a finite element solution. By using a technique described in the references [7, 8], a set of Craig-Bampton modes is solved in the ANSYS [9] finite element code. At first, a set of fixed interface modes and static correction modes are extracted from the FE-model of the part. This set of modes is then orthonormalized and a set of approximate free-free modes and boundary modes is obtained.

Two types of intermediate shafts are used in this study, one with solid circular cross-section and another with hollow circular (i.e. tube) cross-section. Normally straight shafts could be modeled conveniently with beam elements. However, the ADAMS implementation of the floating frame of reference formulation uses lumped mass formulation, in which nodal inertias are neglected. As a result, the rotational inertias are lost when beam elements are used. That is why a solid circular cross-section is modeled with solid elements and a tubular cross-section is modeled with shell elements. By using a dense finite element mesh, the rotational inertias of the body are obtained with a sufficient accuracy. Finite element models of the intermediate shafts are shown in Figure 4. Note that a spider-web mesh of stiff beam elements is used to connect the attachment nodes to surrounding nodes.

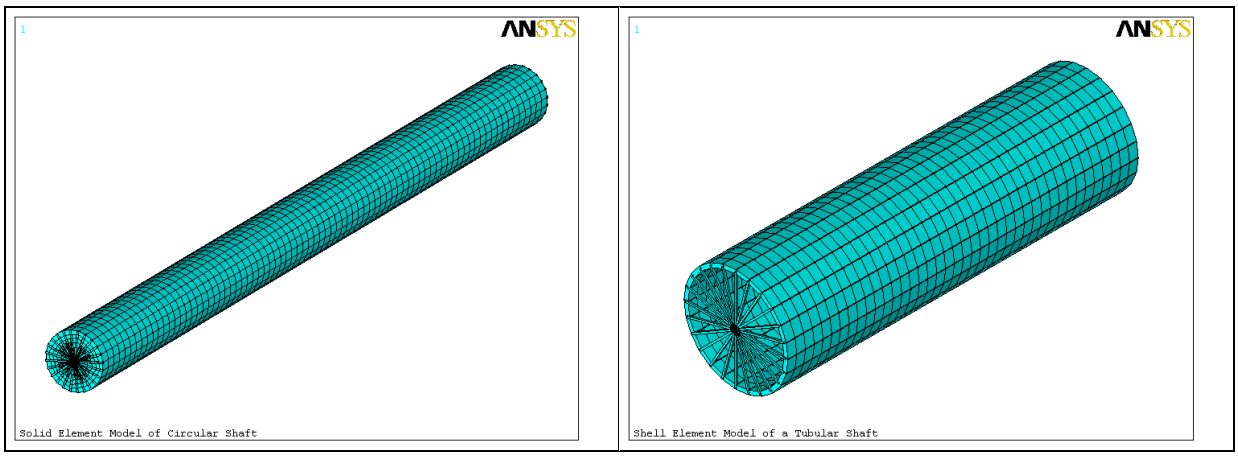

Figure 4. ANSYS finite element models of the intermediate shafts.

3 SIMULATION RESULTS

3.1 Verification of the Analytical Double Cardan Joint Driveline Model

The analytical double cardan joint driveline model presented in section 2.1 is verified with a corresponding ADAMS model, which consists of four parts that are connected with ideal Hooke's joints and a spring force. Rotational inertias of the shafts are: $\{J_1, J_2, J_3, J_4\}$={1.8069e-004, 2.0679e-004, 2.0679e-004, 0.5002} kgm^2 and the torsion spring constant, k_T, is 1.5914e+004 Nm/rad. The damping constant, c_T, is selected to be 1.5914e+002 Nms/rad. Motor torque is defined with the help of the *step* function (see Equation 19) as follows

$$T = 10 \cdot \{step(time, 0, 0, 1.5, 1) + step(time, 1, 0, 3, -1)\} \tag{23}$$

Simulation results are presented in Figures 5 and 6. It can be seen that the agreement between the Matlab/Simulink and ADAMS results is excellent. Small discrepancies in the results are probably caused by different types of numerical integrators. Numerical integrator types and their parameters are shown in Table 1.

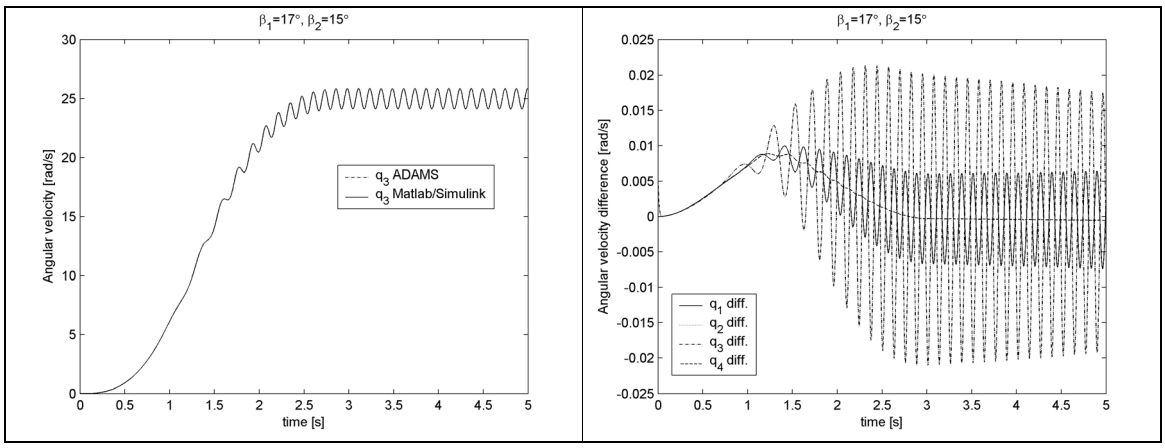

Figure 5. Comparison of Matlab/Simulink and ADAMS models when the joint angles are β_1=17° and β_2=15° and the phase angle is ϕ=90°.

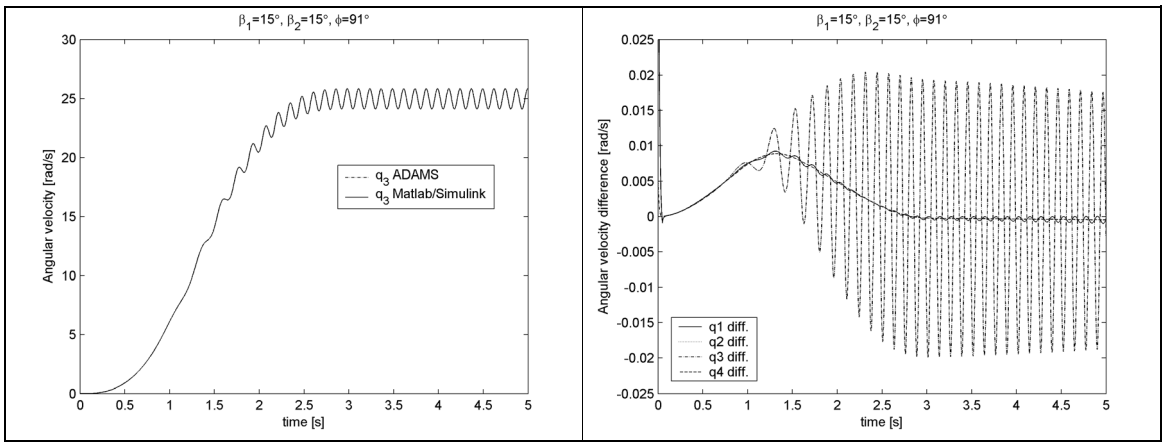

Figure 6. Comparison of Matlab/Simulink and ADAMS models when the joint angles are β_1=15° and β_2=15° and the phase angle is ϕ=91°.

Table 1. Numerical integration parameters.

	Simulink	ADAMS
Integrator	ode15s	Gear stiff
Maximum time step	1.0e-3 sec	1.0e-3 sec
Error tolerance	1.0e-4	1.0e-4
Maximum order	5	6

3.2 Effect of Mechanical Non-idealities on Cardan Transmission Error

Mechanical non-idealities of the double cardan joint driveline are studied in this section. Studied structure is shown in Figure 7. Two universal joints are modeled as described in section 2.2. The motor is driven by a velocity constraint, which could be thought as an ideal motor with unlimited power capacity. For that reason, a very flexible coupling is positioned between the motor and input shaft.

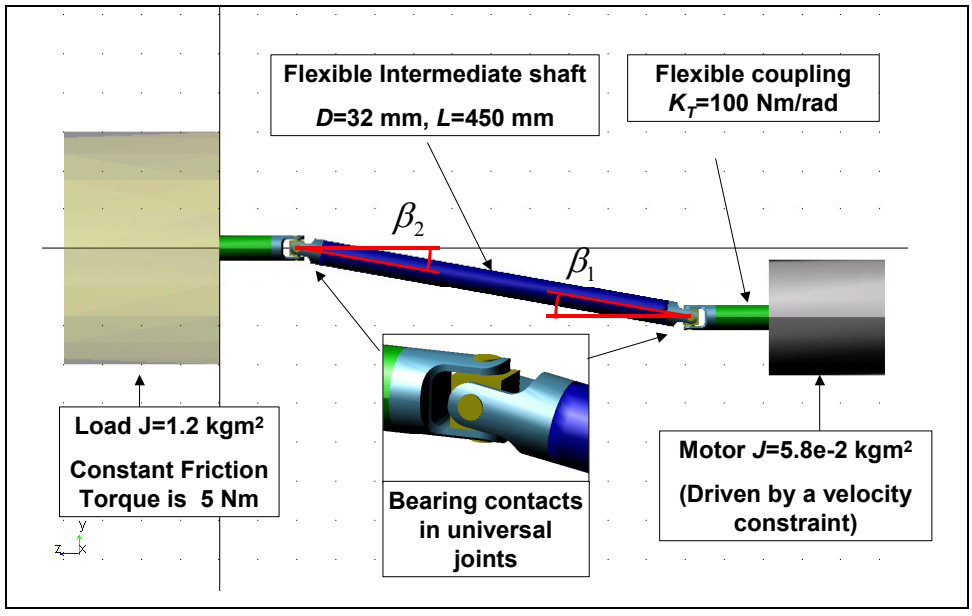

Figure 7. Cardan driveline model.

All parts are made of steel (E = 2.07E+11 N/m^2, ν = 0.3, ρ = 7801 kg/m^3). A total of 15 vibration modes are selected for the intermediate shaft. These modes include 6 bending modes, 6 torsion modes and 3 longitudinal modes. Frequencies of the selected modes range between 710 Hz and 24.4 kHz. Contact parameters for the bearings in the universal joints are as follows:

- Contact stiffness coefficient K = 500 N/μm
- Contact damping coefficient C = 10000 Ns/mm
- Exponent e = 1.5
- Ramp distance d = 10 μm.

The natural frequency of the lowest torsion mode of the system is 19 Hz. The effect of mechanical non-idealities is studied in the following cases:

- CASE 1: A reference case, only bearing contacts and the flexibility of the intermediate shaft are included.
- CASE 2: Misalignment between the input and output shaft is 0.5º.
- CASE 3: The phase angle between the yokes in the intermediate shaft is 0.5º i.e. ϕ = 90.5º.
- CASE 4: All bearings in the universal joints have radial clearance of 20 μm.
- CASE 5: Unbalance mass of 50.0 g is attached in the middle of the intermediate shaft and at the radius of 16 mm.
- CASE 6: The cross part of the output universal joint has a manufacturing error. The centroids of the cross-pins are offset by a distance of 50 μm and, thus, cross-pin axes do not intersect in a common point.
- CASE 7: Misalignment between the input and output shaft is 0.5º and the bearings have a radial clearance of 20 μm.

In all cases the driveline is accelerated from 0 Hz to 15 Hz in 5 seconds and the analysis is continued for 5 more seconds at constant speed. Furthermore, all analyses are run with joint angles of 10 and 20 degrees.

Difference of the rotation speed between the input and output shaft as well as driven torque are used as a measure of cardan driveline transmission error. Spectrum of the input-output speed difference in the constant speed range (5-10s) is shown in Figure 8. The spectrum of the CASE 2 contains peaks at frequencies of even integer multiples of the rotation speed ($2X$, $4X$, $6X$, …). However, the amplitudes of the higher harmonics are negligible compared to $2X$ vibration. For this reason, the amplitude of $2X$ vibration is selected to be a measure of cardan transmission error. The $2X$ amplitudes of speed difference in different cases are shown in Figure 9 and the

corresponding amplitudes of driven torque are shown in Figure 10. It can be seen that the unequal joint angles (CASE 2) cause the most severe vibration. Also the phasing of the joints is important and the second highest amplitudes are found in CASE 3. Bearing clearance in the universal joints increases 2*X* vibration, but the spectrum contains also other frequencies and the level of vibration is increased (see Figure 8). Unbalance of the intermediate shaft (CASE 5) and manufacturing error of the cross part (CASE 6) does not have any effect on torsion vibrations of the driveline.

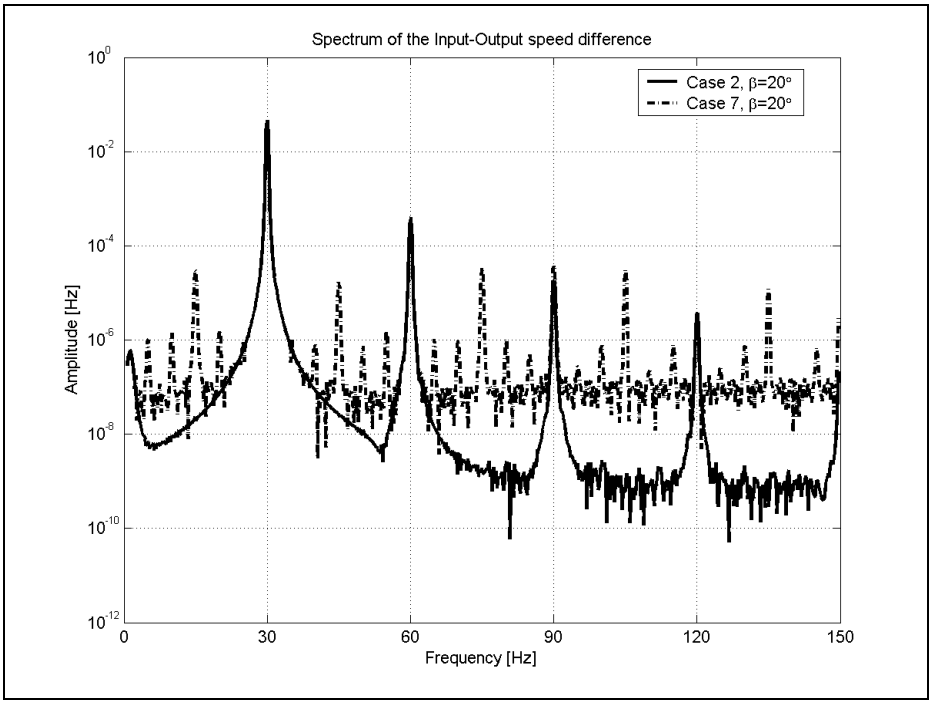

Figure 8. Spectrum of input-output speed difference in Cases 2 and 4.

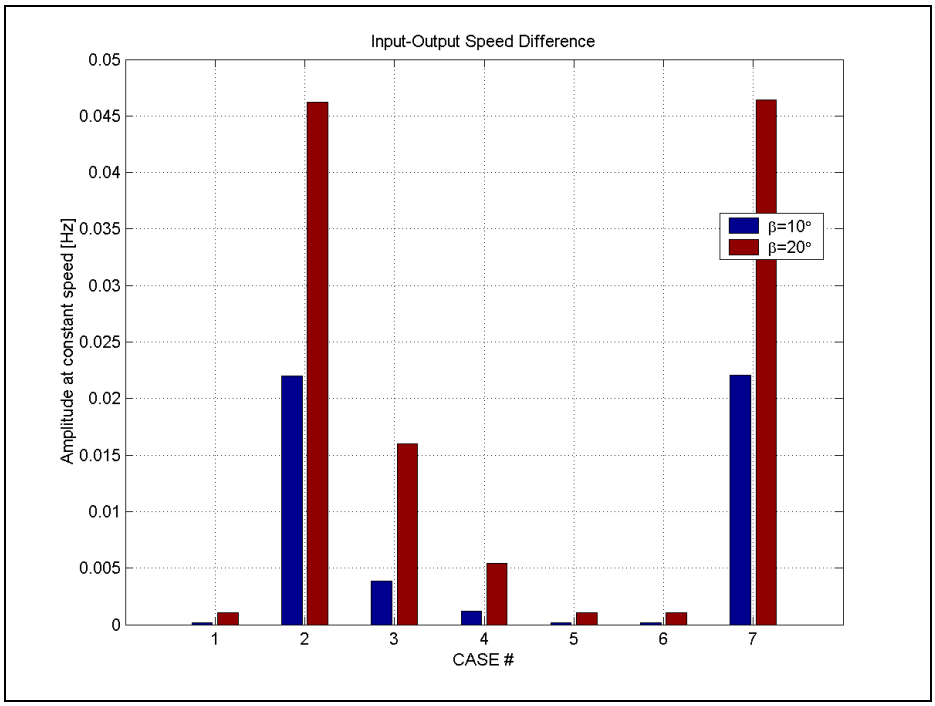

Figure 9. Vibration amplitudes at the frequency of 30 Hz (2X).

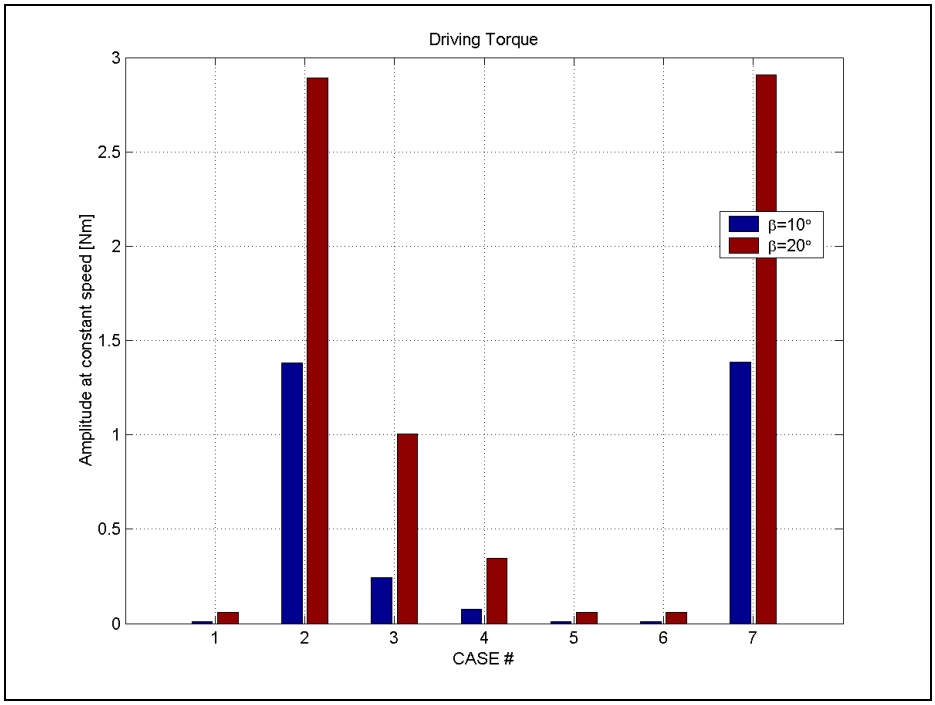

Figure 10. Driving torque amplitudes at the frequency of 30 Hz (2X).

3.3 Co-simulations of Electrical-Mechanical System

Results of coupled electrical-mechanical simulations are presented in this section. The electric motor in this study is a permanent magnet synchronous motor (PMSM). The equations of the motor model can be found in reference [10]. The mechanical system is a double cardan joint driveline with a flexible intermediate shaft. Simulations are performed both in ADAMS and Matlab/Simulink and the obtained results are compared. In the ADAMS model (Figure 11), the

PMSM drive is described as a c-coded subroutine, which is created from the Simulink model of the PMSM using Real-Time Workshop [11]. In the Matlab/Simulink simulations the mechanical system is described as presented in section 2.1. Common parameters for both models are listed in Table 2 and parameter variations in the simulation cases are shown in Table 3. Cases I-IV are analyzed in both programs, but case V is analyzed only in ADAMS, since the bearing clearance is not included in the analytical model of the cardan driveline. In the ADAMS model, 7 vibration modes are selected for the intermediate shaft. These modes include 4 bending modes, 2 torsion modes and 1 longitudinal mode. Frequencies of the selected modes range between 3.4 kHz and 14.8 kHz. Contact parameters for the bearings in the universal joints are the same as listed on page 19. A discrete integrator is used in Simulink and Gear stiff integrator is used in the ADAMS. Time step for both integrators is 12.5 μs.

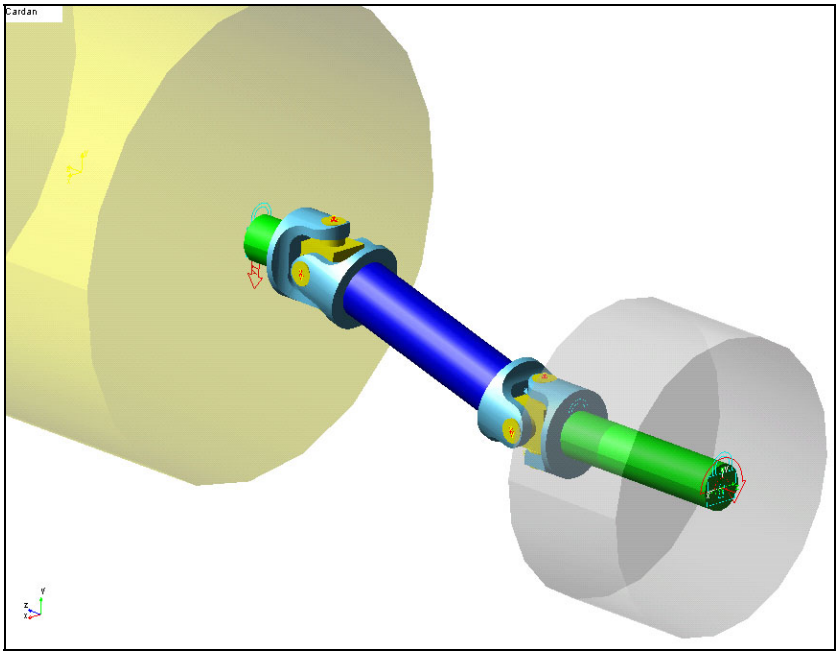

Figure 11. The ADAMS model of the cardan driveline and PMSM.

Table 2. Parameters used in both models.

Moments of inertia $\{J_1, J_2, J_3, J_4\}$	{0.9962, 0.0025, 0.0025, 23.93} kgm^2
Intermediate shaft outer diameter, wall thickness and length	0.0635 m, 0.0040 m, 0.2140 m
Material properties of the parts:	
Young Modulus E	2.07E+011 N/m^2
Poisson's ratio	0.3
Density	7801 kg/m^3

Table 3. Parameter variations in the coupled electrical-mechanical simulations.

Simulation case	Joint angle β_1 [deg]	Joint angle β_2 [deg]	Phase angle ϕ [deg]	Bearing clearance c_d [μm]	Current measurement offset [%]
Case I	15	17	90	0.0	0.0
Case II	15	15	92	0.0	0.0
Case III	15	15	90	0.0	2.0
Case IV	15	17	92	0.0	2.0
Case V	15	15	90	50.0	2.0

The torque of the electric motor and the angular velocities of the shafts in CASE I are presented in Figure 12. The results obtained from ADAMS and Simulink model are in good agreement. Amplitudes of the torque and velocity fluctuations are almost equal, however, some phase shift can be observed. In the ADAMS model, flexibility of the intermediate shaft is described with seven modes and the model includes also the bearing deformation. Therefore, the ADAMS model is more flexible than the Simulink model. The effect of nonlinear bearing forces can be seen in Figure 13, where the angular velocity of the motor at constant reference speed is shown. The angular velocity of the motor is not harmonic in the ADAMS model. The control system of electric motor attempts to compensate the cardan driveline error, which results in a fluctuating torque.

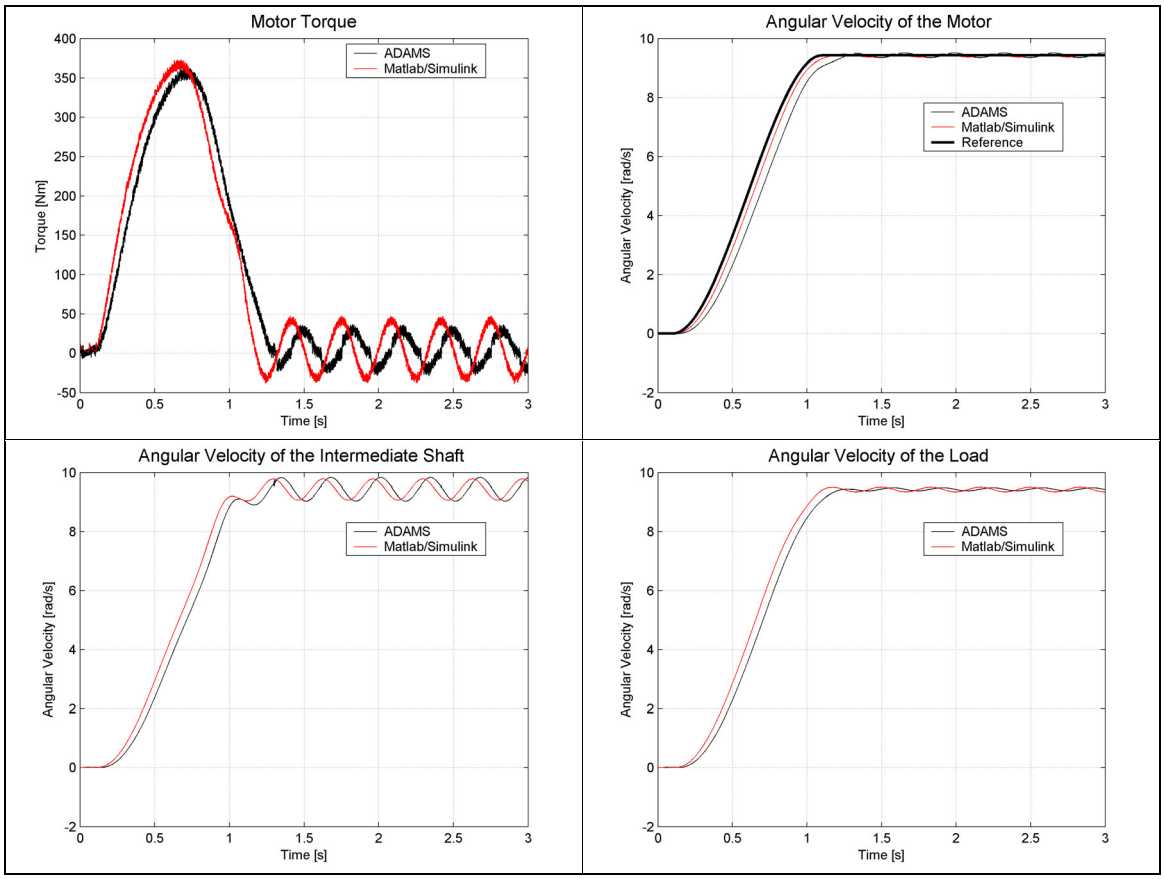

Figure 12. Torque and angular velocities in the CASE I.

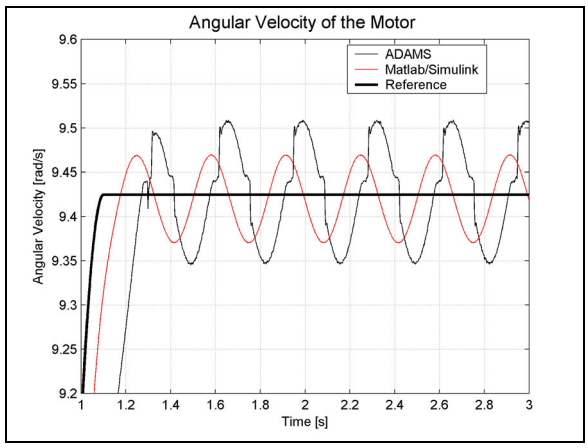

Figure 13. Angular velocity of the motor in the CASE I.

The torques of the electric motor in cases II-V are shown Figure 14 and the angular velocities of the shafts in the corresponding cases are shown in Appendix I. It can be seen that the current measurement error causes vibrations at higher frequency than the mechanical non-idealities. Because of that, these two excitations do not have a dynamical interaction. The effect of the bearing clearance on the torque vibration is small, as can be seen when comparing the results in cases III-V.

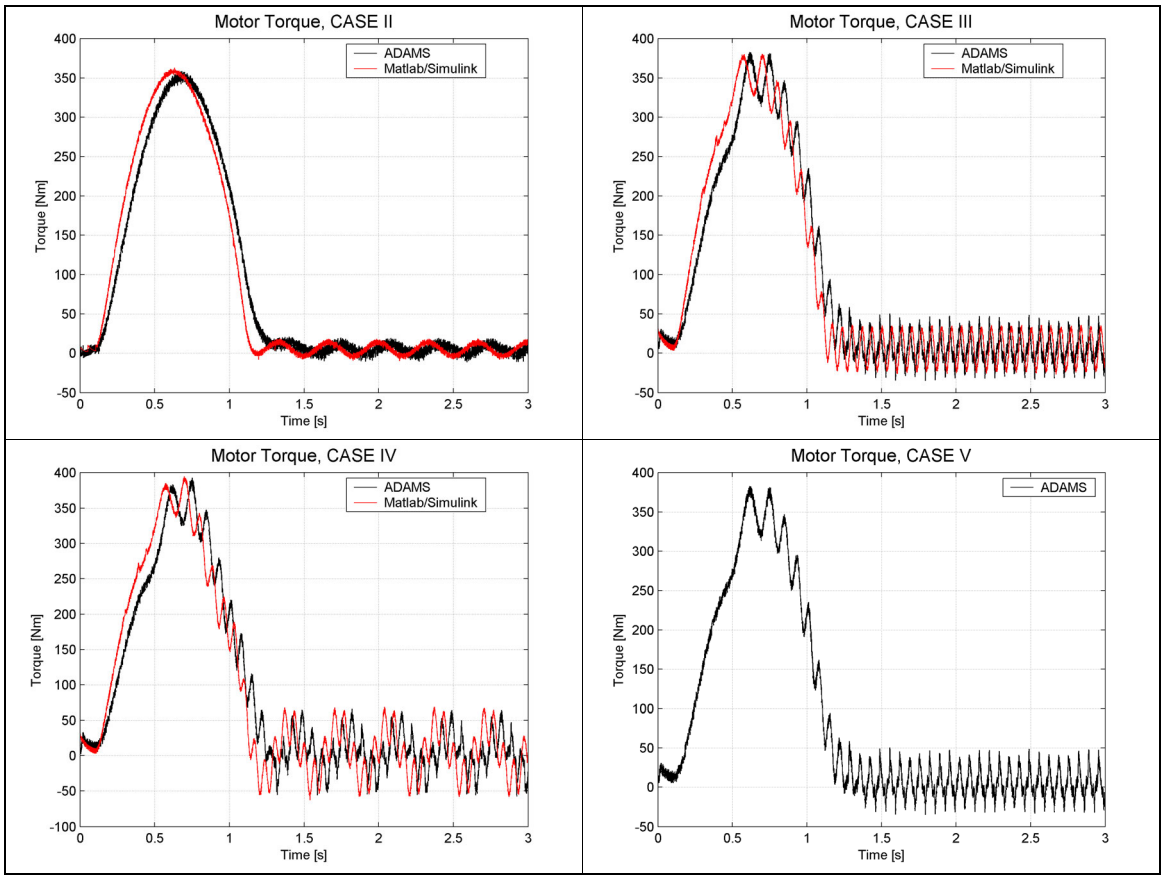

Figure 14. Motor torques in cases II-V.

4 CONCLUSIONS

Two models of the double cardan joint driveline are presented in this study. An analytical model of the driveline is derived using Lagrange's equation and universal joint constraints are described using Lagrange multipliers. The flexibility of the intermediate shaft is described with two masses connected by a spring-damper force. Another model of the driveline is created using a commercial multibody system software application. This model includes descriptions of universal joint bearings forces and the elasticity of the intermediate shaft is described using vibration modes of the shaft. Simulation results between these models are compared and a good agreement is obtained.

Coupled electrical-mechanical analysis of the driveline is performed with a model of permanent magnet synchronous motor (PMSM). The effect of mechanical and electrical non-idealities to the torsion vibration of the driveline is studied with several simulations. The non-idealities include non-ideal cardan joint angles, incorrect phasing of the joints, bearing clearance in the joints and current measurement offset. The simulation results show that the control system of the electric motor tries to compensate the mechanical transmission error of the double cardan joint driveline. This in turn leads to fluctuating torque, which could be avoided either by using a slow control algorithm or by taking the angular velocity of the load into account. In the studied system, the excitation frequencies of the mechanical and electrical systems do not coincide. However, this is not always the case.

REFERENCES

[1] Fischer, I. S., and Paul R. N., 1991, "Kinematic Displacement of a Double-Cardan_Joint Driveline", *ASME Journal of Mechanical Design,* **113**, pp. 263-271.

[2] Sheu, P. P., Shieng, W.H., Lee, A.C., 1996, "Modelling and analysis of the Intermediate Shaft Between Two Universal Joints", *Journal of Vibration and Acoustics,* **118**, pp. 88-99.

[3] Fischer, I. S., and de Waal, J.K., 1995, "Experimental Study of Cardan Joint Dynamics", *ASME Journal of Mechanical Design,* **117**, pp. 526-531.

[4] Brutti, C., Pennestrì, E., Biancolini, M. E., 1999, "On the Dynamics of the Transmission with a Double Cardan Joint", *Tenth World Congress on the Theory of Machine and Mechanisms,* Oulu,Finland, June 20-24.

[5] Shabana, A. A., 1998, Dynamics of Multibody Systems, John Wiley & Sons, New York.

[6] Mancuso, J. R., 1986, Couplings and Joints: Design, Selection, and Application, Marcel Dekker, New York.

[7] Óttarsson, G., 2000, Modal Flexibility Method in ADAMS/FLEX. MDI Technical Paper, Available at: http://support.adams.com/kb/faq.asp?ID=kb7247.dasp.

[8] Craig, R. R., Bampton, M. C. C., 1968, Coupling of Substructures for Dynamic Analyses, AIAA Journal, **6**, pp. 1313-1319.

[9] ANSYS User's Manual, 2001, Theory, Twelfth Edition, SAS IP, Inc. ©.

[10] Vas, P., 1998, Sensorless vector and direct torque control, Oxford University Press, 729 p.

[11] Hirvonen, M., 2003, How to Compile a Simulink model to a ADAMS subroutine using Real-Time Workshop (In Finnish), SAMEKO Project Report, Lappeenranta University of Technology.

APPENDIX I. Angular velocities of the shafts.

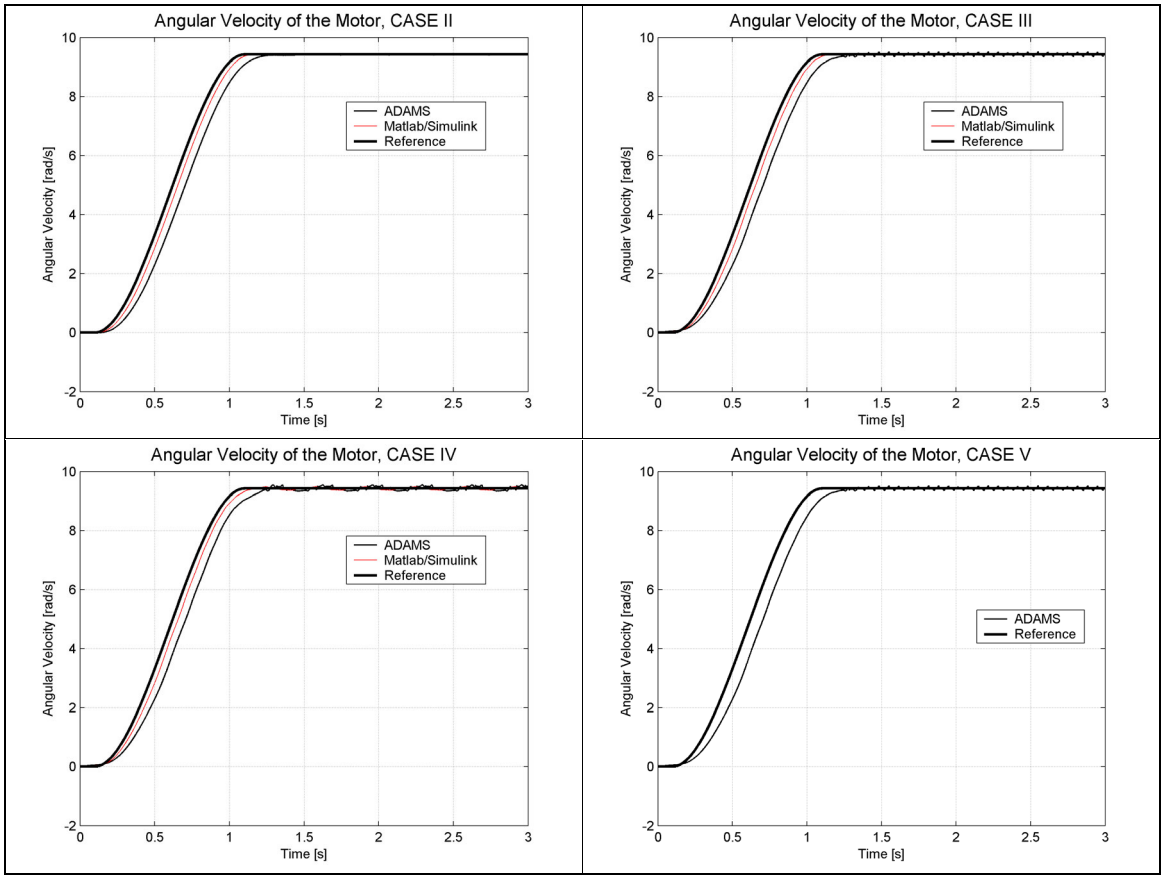

Figure A. 1. Angular velocities of the motor in cases II-V.

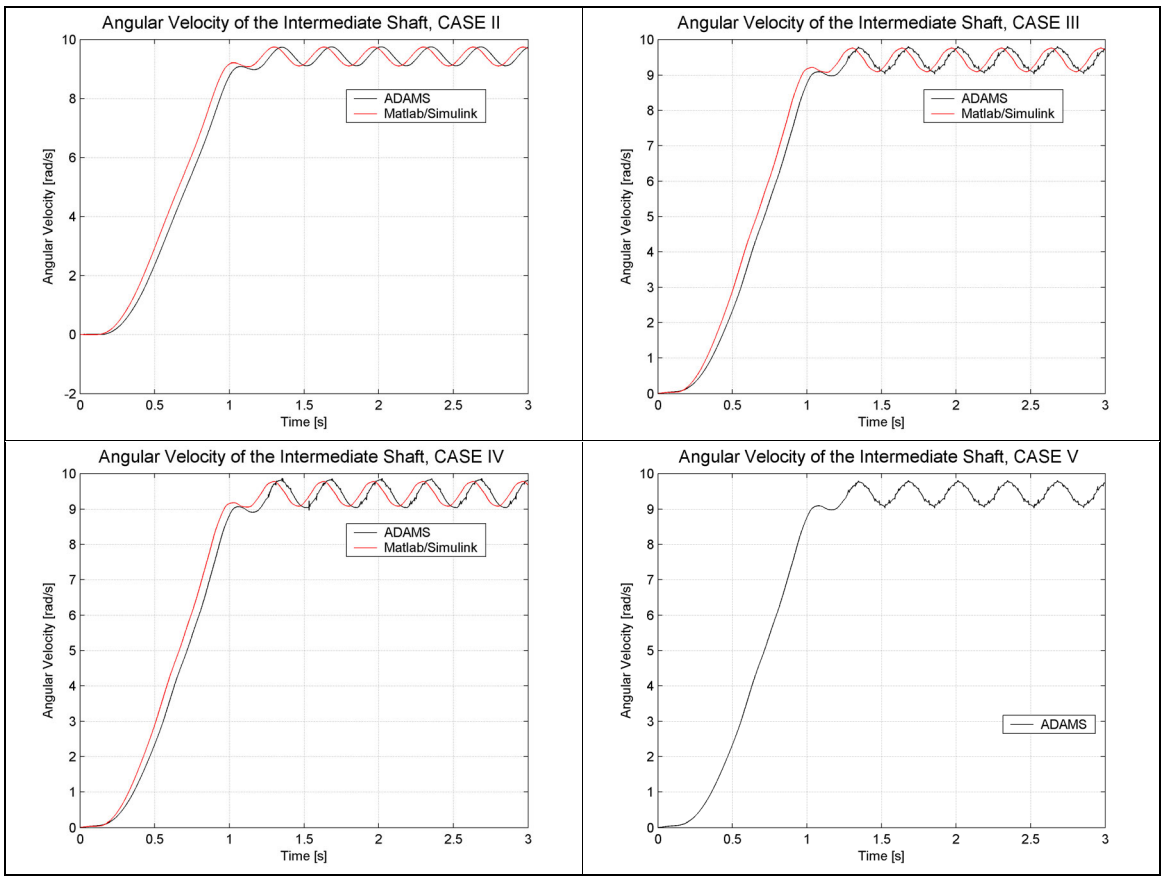

Figure A. 2. Angular velocities of the intermediate shaft in cases II-V.

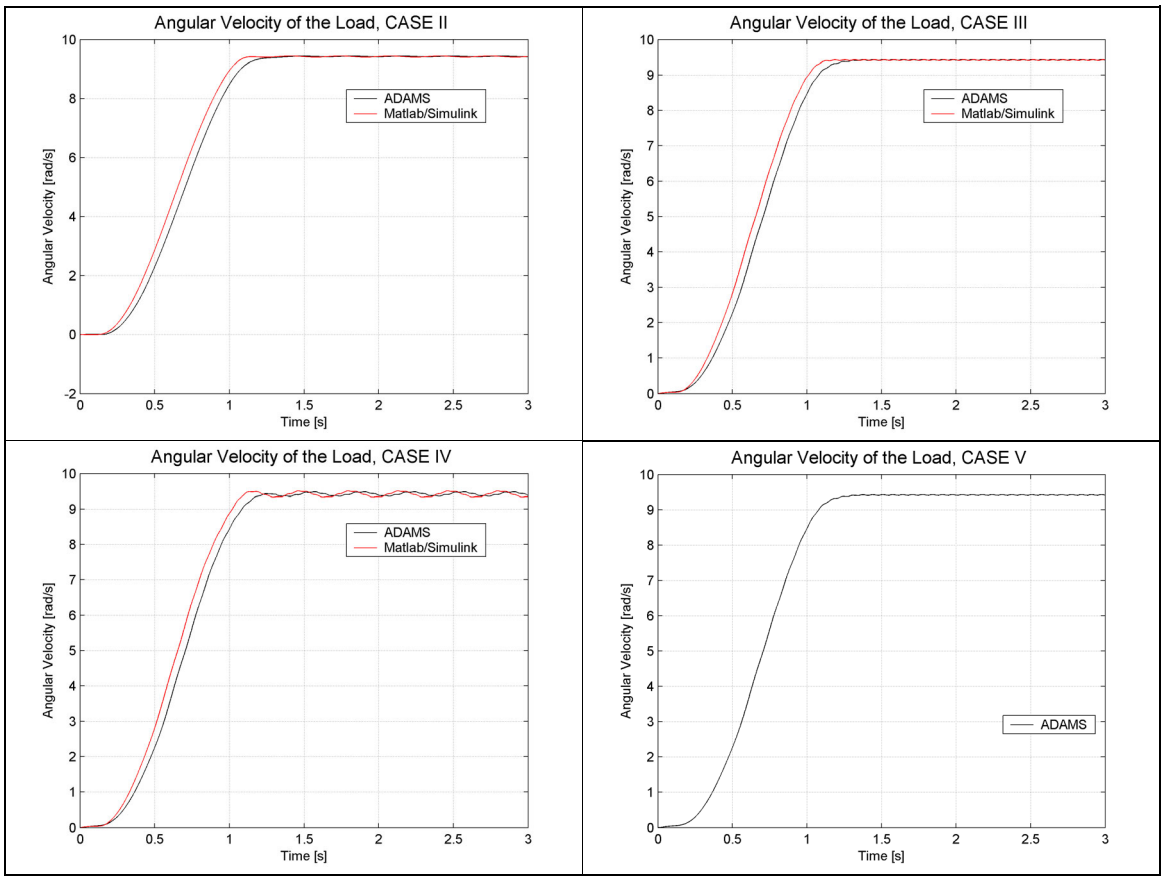

Figure A. 3. Angular velocities of the load in cases II-V.